Atmospheric Pollution Research 7 (2016) 1013–1021

HOSTED BY

ELSEVIER

Contents lists available at ScienceDirect

Atmospheric Pollution Research

journal homepage: http://www.journals.elsevier.com/locate/apr

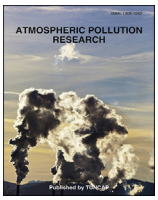

Original article

Features of the annual evolution of CO_2 and CH_4 in the atmosphere of a Mediterranean climate site studied using a nonparametric and a harmonic function

Isidro A. Pérez*, M. Luisa Sánchez, M. Ángeles García, Nuria Pardo

Department of Applied Physics, Faculty of Sciences, University of Valladolid, Paseo de Belén, 7, 47011 Valladolid, Spain

ARTICLE INFO

Article history:
Received 31 March 2016
Received in revised form
13 June 2016
Accepted 18 June 2016
Available online 26 June 2016

Keywords:
Carbon dioxide
Methane
Kernel regression
Harmonic model
South-western Europe

ABSTRACT

Concentrations of CO_2 and CH_4 measured over 3 years at a rural site in the Spanish northern plateau were investigated together with vegetation and meteorological variables. Two procedures were implemented to study the annual evolution. Kernel estimation provided a detailed time description, and the harmonic model may be fitted easily. The site was characterised by grass from autumn to spring. However, vigorous growth was observed during the latter season due to the biological cycle of plants under favourable meteorological conditions. A CO_2 peak was observed a fortnight before the time of maximum NDVI, and was attributed to the prevalence of respiration over photosynthesis. A pronounced trough was apparent in summer and was explained by the death of vegetation and active dispersion in a highly developed boundary layer. CH_4 evolution was characterised by a deficit period from May to October, indicating that meteorological evolution played a key role. The harmonic model showed that annual and half-annual cycles evidenced a similar contribution for CO_2, whereas said weight for the half-annual cycle was considerably smaller for CH_4.

1. Introduction

Greenhouse gases, especially CO_2, have been the focus of research at different sites in an effort to gain insights into their fluxes and evolution, given their link to climate change. Research has recently been conducted in order to establish the contribution of different surfaces and crops to rural CO_2 and CH_4 concentrations (Buragiene et al., 2015; Kim and Kirschbaum, 2015; Luyssaert et al., 2012; Sepulveda-Jauregui et al., 2015). The interest in gaining a detailed knowledge of these gases is widely recognised, since they are measured by an extensive network whose observations are distributed worldwide by international databases such as the World Data Centre for Greenhouse Gases (WDCGG) and corresponding publications (WDCGG, 2016). Moreover, the impact of their increasing concentrations on crops has been quantified (Saha et al., 2015). However, academic papers addressing their current levels are usually confined to urban environments where combustions are the main sources (Hernández-Paniagua et al., 2015), whereas campaigns at rural sites focus on background concentration measurement (Cheng et al., 2013; Pu et al., 2014).

The present paper focuses on the annual cycle of both gases in the atmosphere, which may be considered a fingerprint of the site where measurements are obtained. This is a specific feature of the present research, since studies exclusively devoted to analysing annual evolution remain infrequent and normally appear together with research into the temporal trend (Artuso et al., 2007; Liu et al., 2015; Zhu and Yoshikawa-Inoue, 2015). When trend values are much lower than the annual range, analysis may exclude the trend and focus on the annual evolution.

The influence of the ecosystem has been the focus of CO_2 and CH_4 research (Boeckx and Van Cleemput, 2001; Evrendilek et al., 2005). Hence, gas concentration may be accompanied by vegetation data provided by satellite (Myneni et al., 1998; Tucker et al., 2001). Moreover, meteorological variables, such as the boundary layer height, prove necessary to obtain information concerning atmospheric dispersion.

The current study first deals with the procedure to analyse the yearly cycle. Since short time processes can hide slow changes,

* Corresponding author. Tel.: +34 983 184 189; fax: +34 983 423 013.
E-mail address: iaperez@fa1.uva.es (I.A. Pérez).

Peer review under responsibility of Turkish National Committee for Air Pollution Research and Control.

http://dx.doi.org/10.1016/j.apr.2016.06.006

smoothing procedures must be considered when investigating the annual pattern. Similar methods have been used in trend analyses. Thoning et al. (1989) smoothed CO_2 observations at Mauna Loa by filtering the daily averages with a low-pass filter. The same technique was applied by Bakwin et al. (1995) to four background sites. Finally, Bakwin et al. (1998) smoothed CO_2 observations in North Carolina from 1992 to 1997 and Wisconsin from 1994 to 1997 with a second order polynomial and four seasonal harmonics.

Tiwari et al. (2013) fitted the observed CO_2 concentrations over Cape Rama, on the west coast of India using a nine-degree polynomial. Their procedure provided smoothed concentrations. However, the successful description of concentrations obtained by increasing the degree of the polynomial is counterbalanced by the gap observed at the end of the year. Concentrations were nearly 1 ppm lower than those at the beginning, with this gap being around 10% of the interval presented. This problem linked to circular variables was evidenced by Anderson-Cook and Noble (2001), who employed quadratic and cubic models, centring the curves in the data and placing the discontinuity away from the observations. However, uniformly distributed measurements make such models inadvisable. The present paper presents two alternative methods to overcome this drawback. The first is based on the kernel estimation and the second on the second order model for cylindrical data. Both methods do not need specific requirements to be implemented and may be extended to other places to explain the behaviour of circular variables such as daily cycles or directional analyses (Pérez et al., 2007).

The first procedure based on nonparametric regression was successfully used to investigate point and linear sources of air pollution (Henry et al., 2002, 2011). This paper discusses the limits of this technique when used to study annual evolution. As a specific feature, its low restrictions provide a detailed analysis of the number and duration of periods of excess and deficit compared to the average concentration.

The second procedure is a harmonic analysis. Nakazawa et al. (1997) and Tans et al. (1989) used an addition of polynomic and harmonic functions to investigate CO_2 evolution. This method should be observed as a first step towards describing the evolution of an atmospheric variable. However, experience has shown that a low number of harmonics may also be satisfactory (Artuso et al., 2009). The current paper considers a model based on only two harmonics, whose suitability is analysed. Moreover, amplitudes and phase constants may determine the weight of harmonics and the features of the evolution.

A second objective of this paper is the relationship between data presented and similar studies. Although the Mauna Loa observations have been widely analysed, the yearly cycle of both trace gases recorded at different sites has been considered in several papers. Once the yearly pattern is established at the measurement site, the ranges and times of noticeable concentrations are determined and compared with those measured in other places, mainly in Europe and Asia, which are representative of varied climates, in order to explore yearly patterns and to determine sites whose observations may be considered as outliers.

Finally, the database employed in this paper is far more extensive than those previously used, and the procedures carried out have not to date been considered at this semi-natural site, where research had focused on CO_2 contrast with an urban location (García et al., 2012), CO_2 cluster analysis (Pérez et al., 2015a), and the study of CH_4 measurements (Sánchez et al., 2014).

2. Materials and methods

2.1. Experimental description

The measurement campaign extended over three years (15 Oct. 2010–14 Oct. 2013) at the Low Atmosphere Research Centre (CIBA) (41º 48′ 50.25″ N, 4º 55′ 58.56″ W, 850 m a.s.l.), Fig. 1(a). Vegetation at the site comprises Mediterranean scrubland which stretches at least 50 m from the measurement site. The rest is formed by non-irrigated crops and a small group of pine-trees some 200 m to the SW, Fig. 1(b). Potential emission sources are not present in the close vicinity of the measurement site.

CO_2 and CH_4 dry mole fractions continuously measured in ppm were supplied by a Picarro G1301 analyser, which is based on cavity ring-down spectroscopy. In this technique, a gas sample is

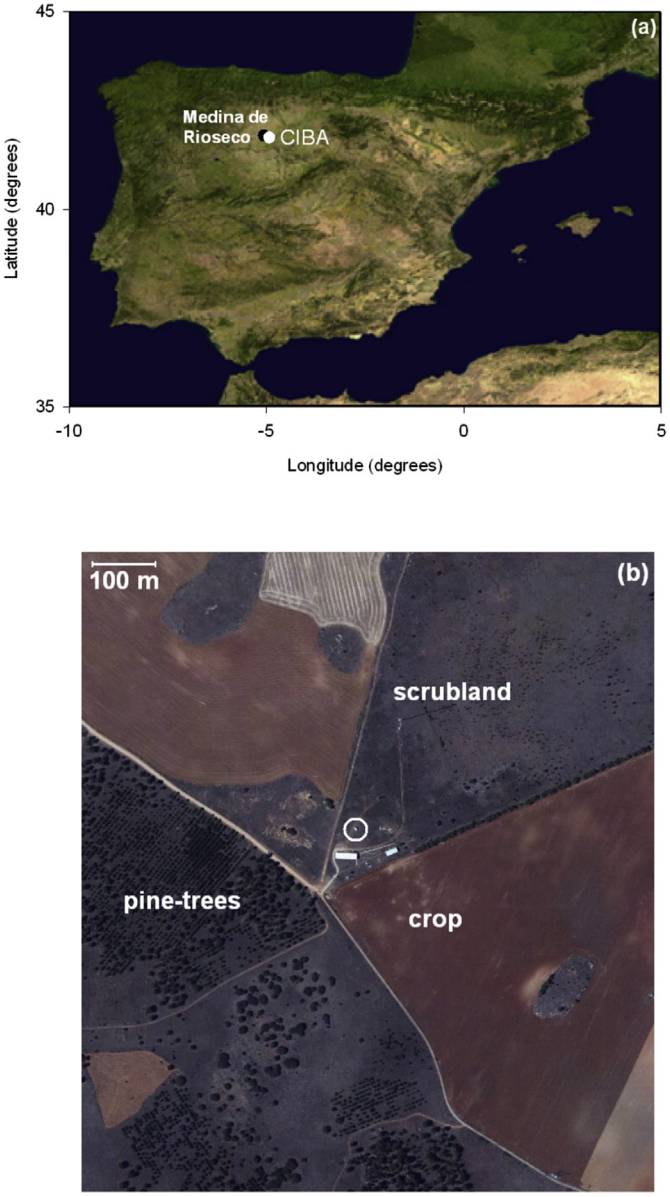

Fig. 1. (a) NASA image showing the measurement site as a white dot, CIBA, and the meteorological station as a black dot, Medina de Rioseco, located on the northern plateau of the Iberian Peninsula. (b) PNOA image courtesy of © ign.es showing the land use around the measurement site, marked with the white ring.

introduced into a high-finesse optical cavity. Light from a laser is injected into the cavity and is monitored with a photo-detector. The "ring-down" measurement is made when the laser is turned off and the decay of the light intensity is measured. This decay depends on the losses by the cavity mirrors and the absorption and scattering of the sample (Crosson, 2008). This monitor achieves the WMO inter-laboratory comparability standard for both gases without drying the sample gas (Chen et al., 2010; Rella, 2010; Rella et al., 2013). The manufacturer indicates that the device's precision was 0.2 ppm for CO_2 and 0.001 ppm for CH_4. Around 30 measurements were made each minute and were recorded at three levels; 1.8, 3.7 and 8.3 m, through solenoid valves controlled by the analyser. These levels follow a logarithmic scale, which is frequent in micrometeorology, and were selected to investigate the behaviour of both gases close to the ground surface. Measurements lasted 10 min at each level and the first 20 observations were not considered in order to avoid discontinuities when the level changed. However, values supplied by this device were averaged on a semi-hourly basis. Calibrations were performed each two weeks with three NOAA standards of values presented in Table 1, which are above, around and below the background concentrations. The temporal length of the calibration injection was about 5 min for each gas. The device is extremely stable, since its coefficients of variation calculated with measurements of calibrations over the three years were around 0.04% for CO_2 and 0.19% for CH_4. Calibrations were used to slightly correct the measurements by employing the following linear equations:

$$CO_{2\,C} = 1.00369\,CO_2 - 0.22882, \tag{1}$$

$$CH_{4\,C} = 0.99321\,CH_4 + 0.01206, \tag{2}$$

where the C subscript corresponds to the corrected value. Equation (1) represents a slight correction of the expression used by Pérez et al. (2013) for two years of measurements.

One noticeable feature of the current paper is that meteorological measurements were obtained from the METEX model (Zeng et al., 2010) by using NCEP re-analysis as the data set. Although this is a model for air mass trajectory calculation, ancillary variables were also provided. In this paper, only boundary layer height, temperature and wind speed were used. The wind speed and direction provided by this model showed similar values to those measured, although prevailing directions were less marked by the model than for observations (Pérez et al., 2015b).

Since the METEX model provides values on an hourly basis, arithmetic means of concentrations were calculated to make them compatible with meteorological variables. Availability of hourly concentration was about 95% of possible observations at the levels investigated, with August 2013 being the most noticeable gap recorded in concentration.

NDVI values were used to quantify vegetation evolution, and were obtained from MODIS at the TERRA satellite and downloaded from EOSDIS Reverb (NASA, 2016).

Daily precipitation observations were downloaded from the meteorological station at Medina de Rioseco (41° 51′ 38.75″ N, 5° 4′ 14.44″ W, 739 m a.s.l.), supported by the Ministry of Agriculture, Food and Environment, and nearly 12.6 km NW of the CIBA, Fig. 1(a) (MAGRAMA, 2016).

Table 1
NOAA standards used in periodical calibrations.

Standard	CO_2 (ppm)	CH_4 (ppm)
1	452.56	1.9904
2	399.27	1.8420
3	348.55	1.6310

2.2. Kernel estimation

This procedure allows for calculations of locally weighted averages over a sliding window of width h (Donnelly et al., 2011; Henry et al., 2002). Greater weight is given to concentrations C_i observed at times t_i that are close to time t where the weighted average $C(t,h)$ is calculated and less weight is attached to distant observations, following the equation

$$C(t,h) = \frac{\sum_{i=1}^{n} K\left(\frac{t-t_i}{h}\right) C_i}{\sum_{i=1}^{n} K\left(\frac{t-t_i}{h}\right)}, \tag{3}$$

where n is the number of observations.

The preferred function K used to weight observations of circular data is the Gaussian kernel, described by

$$K(x) = (2\pi)^{-1/2} \exp\left(-0.5x^2\right) \quad -\infty < x < \infty \tag{4}$$

2.3. Second order model for cylindrical data

Anderson-Cook (2000) presented this model, which was adapted following the equation

$$C_i = a + b\cos(2\pi(t_i - \theta_1)) + c\cos(4\pi(t_i - \theta_2)), \tag{5}$$

where t_i, θ_1 and θ_2 are times measured as a fraction of the year, and the range for θ_1 is 1 corresponding to one year and for θ_2 is 0.5 corresponding to half of the year. The a, b and c parameters are calculated by transforming Eq. (5) into

$$C_i = a + b_1\cos(2\pi t_i) + b_2\sin(2\pi t_i) + c_1\cos(4\pi t_i) + c_2\sin(4\pi t_i). \tag{6}$$

Parameters of this equation may be determined by multiple linear regression, and allow parameters of Eq. (5) to be calculated by means of

$$b = \sqrt{b_1^2 + b_2^2};\ \theta_1 = \frac{atan\left(\frac{b_2}{b_1}\right)}{2\pi};\ c = \sqrt{c_1^2 + c_2^2};\theta_2 = \frac{atan\left(\frac{c_2}{c_1}\right)}{4\pi} \tag{7}$$

3. Results and discussion

Fig. 2 shows that the hourly concentrations recorded at the three levels were very homogeneous. They were slightly lower for CO_2 at the third level than at the first. However, the behaviour was the opposite for CH_4. The vertical gradients obtained by $(C_{8.3\ m} - C_{1.8\ m})/(8.3\ m - 1.8\ m)$ were −3.5 and 0.0016 ppm in 10 m, respectively, and are only valid in the layer where observations were measured.

3.1. Kernel estimation

Although Eq. (3) with the kernel given by Eq. (4) considers all observations, one problem which arises prior to applying this procedure concerns proposing the window width, h. A narrow window gives great weight to the neighbouring observations, perhaps causing sharp changes, while a wide window may lead to

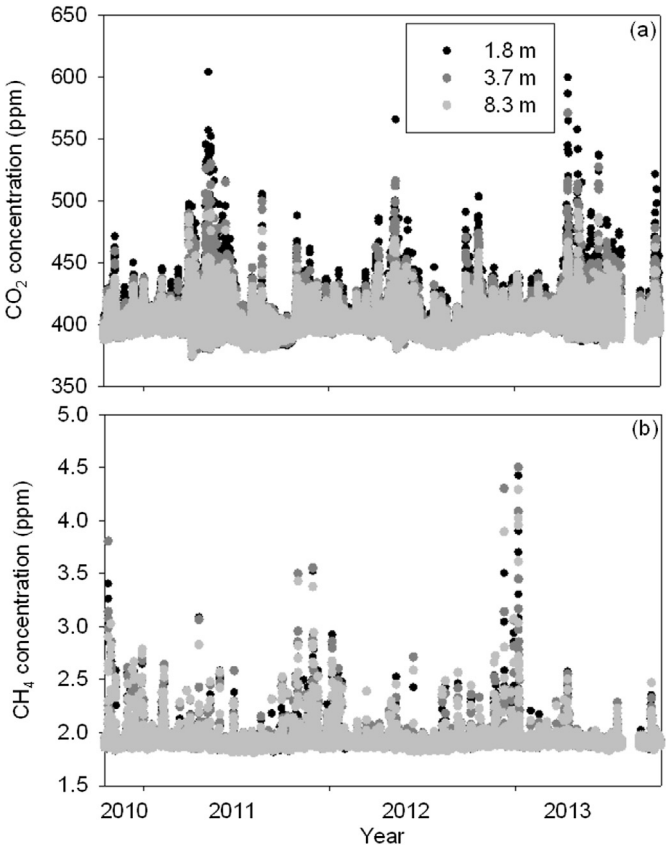

Fig. 2. Scatter plot showing the hourly series of observations at the three levels considered, (a) for CO_2 and (b) for CH_4.

significant smoothing that masks the behaviour at certain scales (Pérez et al., 2007). Therefore, although Donnelly et al. (2011) considered a method based on the standard deviation of the data for choosing the window width, this procedure was not applied in this research since a uniformly distributed circular variable, namely time, is used. One desirable property in this analysis for the window width is that it should provide information about monthly changes. Although the greatest weight of Eq. (4) was obtained for $t = t_i$, it decreased quickly. Two groups of variables were formed. One 10-day window was used to retain certain fluctuations with CO_2, NDVI, temperature and boundary layer height. The weight of this window was about one percent of the maximum from 30 days before the day of calculation to 30 days after the day of calculation. Another slightly larger window, 15 days, was used for CH_4 and wind speed to smooth oscillations of these variables that evidence rapid changes. In this case, the period of greatest weight extended to around 45 days from the day of calculation. With these windows, oscillations are not noticeable in the two groups of variables and monthly changes are retained.

Equation (3) was used to describe the annual evolution of both trace gases, by calculating one value each day. Fig. 3(a) presents CO_2 evolution at 8.3 m, with the average concentration at 1.8 m being around 2.3 ppm higher. The smoothed curves were similar for the three levels, with the highest concentration being 4.8 ppm lower at 8.3 m than at 1.8 m, while the minimum was only 1.4 ppm lower. The mean percentage difference between observations and smoothed values was 1.4% for the highest level and 2.1% for the lowest. Calculations with windows from 5 to 20 days revealed a similar model response for these mean percentage differences.

The climate at the site is temperate without a dry season, and with a temperate summer, Cfb, following the Köppen-Geiger classification (Atlas Agroclimático de Castilla y León-ITACYL-AEMET, 2013). Smoothed temperature revealed a gradual increase from 3 °C at the beginning of February to 20.3 °C in mid August, Fig. 3(b). Monthly averaged precipitations showed a mean value of 34.2 mm. They are irregularly distributed and two periods may be observed, Fig 3(c). Precipitation was continuously below this value from May to September, due to convective showers. However, it was mainly above the mean during the rest of the year, and was attributed to fronts sweeping the peninsula, mainly from the West. The boundary layer developed from 250 m at night to maximum values during the day. Smoothed values ranged from 350 m in winter to around 950 m in summer, Fig. 3(d). Smoothed wind speed reached the highest values in November–February, around 6 m s^{-1}, but decreased slowly until August, reaching around 3.5 m s^{-1}, Fig. 3(e). Metzger et al. (2005) considered 84 environmental strata (following climate data, data on the ocean influence, and geographical position), which were grouped into 13 environmental zones. The site was labelled as Mediterranean North, with the maximum precipitation in winter, dry summer, and growing season lasting 335 days (Wageningen UR, 2016).

NDVI quantifies plant growth. Table 2 was built from values described by the Mapping and Geological Institute of Catalonia (ICGC, 2016), which are similar to those from NASA (2000), to easily explain the annual evolution smoothed in Fig. 3(f). Grass is the main vegetation during most of the year, from early July to late March. However, abundant and vigorous vegetation is observed in spring with a peak in late May. Pérez-Hoyos et al. (2014) presented a classification with 12 Ecosystem Functional Types (EFTs), which was applied to Spain. According to this classification, the measuring site corresponds to the second type, described by a high albedo attributed to the low density of the crop canopy, which determined a strong influence of soil. Averaged NDVI was 0.38, with a spring peak and high intra-annual variability.

The average CO_2 value was 399.1 ppm, in agreement with flask data (NOAA, 2016), and allowed two periods to be established. CO_2 excess prevailed during the first period, from late October to mid June, with a deficit being noticeable during the second period, in summer and early autumn. This evolution agrees with the vegetation cycle. During autumn and winter, precipitation and low temperatures ensure grass at the site, with plant respiration being responsible for CO_2 values around 2 ppm above the mean, according to Fig. 3(a). Precipitation and higher temperature in early spring led to vegetation development, which is reflected in increased NDVI values. Consequently, CO_2 increased, probably due to respiration processes and background evolution during this period of intense activity, reaching a maximum in early May. However, vegetation growth also determined intense photosynthesis during the daylight period, which lasted over 14 h in May and 15 h in June. This sharp contrast between daytime and night time periods is presented in Fig. 4(a), where major differences of around 17 ppm were reached in spring, while the differences between the two periods in the rest of the year remained below 5 ppm. Expansion of the boundary layer together with photosynthesis thus accounted for the lack of agreement between CO_2 and NDVI peaks, with vigorous vegetation and long days in late May and early June. When vegetation declined in early July, its respiration and photosynthesis also decreased. Another contributing factor in this period was intense dispersion of a thermal origin linked to high temperatures and low mechanical turbulence due to low wind speed. Under these conditions, the boundary layer expanded substantially and dilution increased (Pérez et al., 2012). Together with the background evolution, these factors might determine CO_2 decrease. The minimum values reached in late August might be justified by the extremely weak plant activity. Precipitation in early autumn

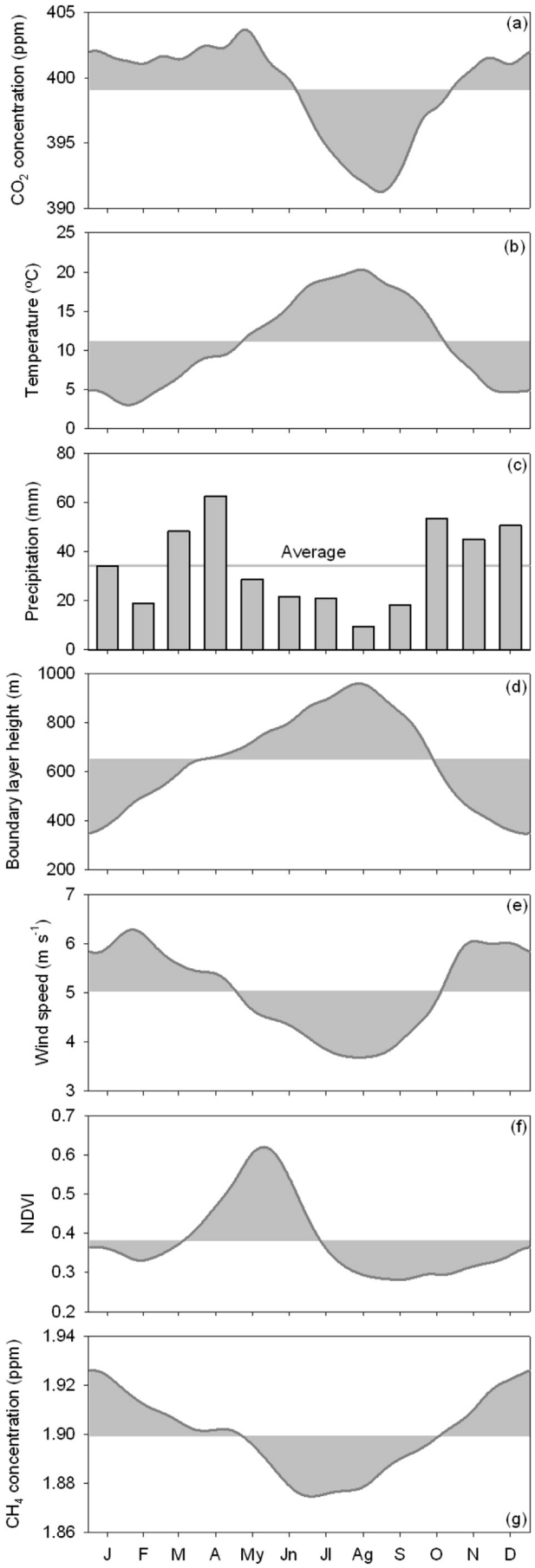

Table 2
Vegetation types following NDVI values.

NDVI	Vegetation
0–0.2	Bare soil and dead vegetation
0.2–0.4	Shrub or grassland
0.4–0.6	Abundant and vigorous vegetation
>0.6	Very dense and vigorous vegetation

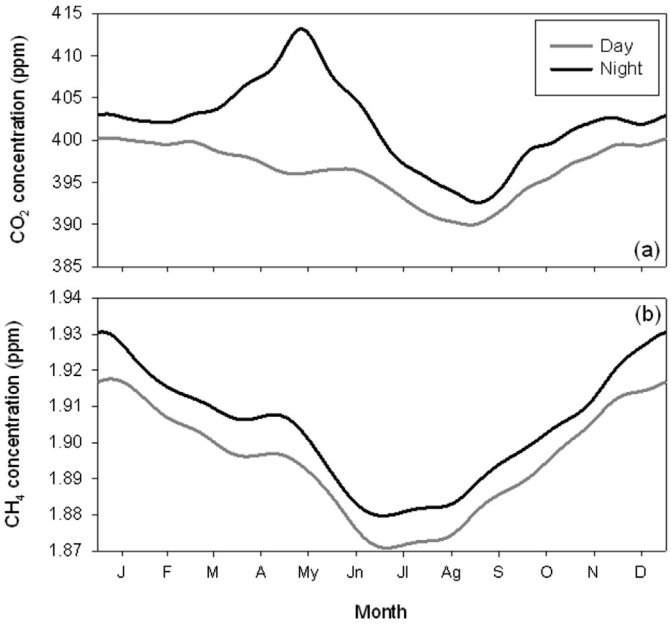

Fig. 4. Yearly patterns of CO_2 (a) and CH_4 (b) concentrations during daytime and night time.

explained the gradual development of light vegetation accompanied by increasing plant respiration.

Table 3 presents the main details at different places where this evolution was observed. Although measurement conditions are very varied, the yearly pattern involves one maximum and one minimum, with noticeable features being the months these values were attained and the range between them. At most of the sites, maximum values occurred in March–April. Singular cases were Hegyhátsál (Hungary) and Cabaw (The Netherlands), which displayed maxima in December and January, respectively. Moreover, both places present the greatest ranges, above 20 ppm. Minima were mainly observed in August, with noticeable exceptions being Mauna Loa (Hawaii), whose minimum was in October, and Cape Rama (India), in November. Excluding the analysis of Tian et al. (2014), which involves different sites, the lowest range was observed at Mauna Loa, with only 6 ppm.

The annual CO_2 evolution at CIBA, with a maximum in May, a minimum in August and a range of around 13 ppm, may be observed as a fingerprint that allows the site atmosphere to be identified. According to these features, this evolution agrees with Tsukuba (Japan) or Alert (Canada).

Annual CH_4 evolution at the site is shown in Fig. 3(g) by a simple oscillation, with a maximum in winter and a minimum in summer and a range of about 0.05 ppm. The average concentration was

Fig. 3. Annual evolution smoothed with a Gaussian kernel in a dark grey line and differences with the average filled in using light grey for the variables (a) CO_2, (b) temperature, (d) boundary layer height, (e) wind speed, (f) NDVI and (g) CH_4. A bar chart was used for precipitation (c).

Table 3
Sites where annual atmospheric CO_2 evolution was investigated, with the main features.

Paper	Site and height a.s.l. (m)	Month (maximum)	Month (minimum)	Range (ppm)	Measurement height (m)	Climate pattern	Underlying surface
Eneroth et al. (2005)	Pallas, northern Finland, 565	February	August	15–20	7	Subarctic	Low vascular plants, moss and lichen
Haszpra et al. (2008)	Hegyhátsál, Hungary, 248	December	August	30	10	Temperate continental	Agricultural fields, pastures and forest patches
Higuchi et al. (2003)	Cold Bay, Alaska, 21	April	August	13	Flask	Subpolar oceanic	
	Fraserdale, Canada, 210	March–April	August	20	40	Boreal forest	Tall grass and small willow trees
	Alert, Canada, 200	May	August–September	15	Flask	Polar tundra	Ice, slate and shale
Inoue et al. (2006)	Tsukuba, central Japan, 25	April	August	12	200	Temperate without dry season	Grass
Lintner et al. (2006)	Mauna Loa, Hawaii, 3397	May	October	6	7–27	High mountain	
Tian et al. (2014)	Varied environments	April	August	4			
Tiwari et al. (2013)	Cape Rama, India, 60	March	November	<8	6 (flask)	Monsoon	Free of vegetation
Uglietti et al. (2011)	Jungfraujoch, Switzerland, 3580	March	August	8.7	15	High mountain	Rock
Vermeulen et al. (2011)	Cabaw, The Netherlands, −0.7	January	August	<25	20–200	Atlantic with soft summer	Intensively and extensively managed grassland
Wada et al. (2007)	Minamitorishima, western North Pacific, 9	April–May	September	7	10	Tropical savanna	
Zhou et al. (2005)	Mount Waliguan, China, 3816	April	August	10	5 (flask)-80	High mountain	Sparse vegetation, arid grassland and desert

1.899 ppm, which was in agreement with flask data (NOAA, 2016), and was 0.001 ppm lower for the 1.8 m level. Mean percentage differences between observations and smoothed values were 1.4% for the three levels and nearly insensitive for windows from 5 to 20 days. Excess prevailed from October to April, and there was a deficit during the rest of the year. CH_4 evolutions for the three levels were similar and seemed to be anti-correlated with the mixing height and, in some way, correlated with wind speed. This behaviour revealed that dispersion processes in the low atmosphere played a major role in concentration evolution. Fig. 4(b) shows the daytime and night-time evolutions. Unlike CO_2, CH_4 concentration during the night was regularly higher than during the day, around 0.009 ppm, due to the stable stratification of the low atmosphere in this period. Sánchez et al. (2014) presented the annual evolution at the same site for the period June 2010–May 2012 by monthly means. Although similar, the range was about 0.06 ppm and the trough was more pronounced than in Fig. 3(g).

Table 4 presents the features of the CH_4 yearly cycle as well as details concerning its measurement at different sites. One maximum and one minimum value are usual. However, noticeable exceptions are the evolution observed on the Tae-ahn Peninsula, Korea, which evidenced changing values (Kim et al., 2015) and the yearly cycle at Schneefernerhaus, Germany, where maxima were found in April and August, and where minima were observed in June and November (Zhang et al., 2013). Moreover, noticeable differences are observed at Mt. Waliguan, China, where most studies presented ranges of around 0.01 ppm, except Kong et al. (2010), who depicted a range of 0.04 ppm taken from Liu et al. (2004). Noticeable ranges, reaching up to 0.1 ppm, the greatest amongst those observed in the other places considered, were obtained at Hegyhátsál in Hungary, and Cabaw in The Netherlands. The yearly cycle at the measurement site was similar to most of those reported, although the concentration range was intermediate.

Table 4
Sites where annual atmospheric CH_4 evolution was investigated, with the main features.

Paper	Site and height a.s.l. (m)	Month (maximum)	Month (minimum)	Range (ppm)	Measurement height (m)	Climate pattern	Underlying surface
Artuso et al. (2007)	Lampedusa, Italy, 45	February–March	August	0.03	3	Semi-arid	Rocky, poor in vegetation
Haszpra et al. (2011)	Hegyhátsál, Hungary, 248	December–January	July	0.1	96	Temperate continental	Agricultural fields, pastures and forest patches
Kim et al. (2015)	Mt. Waliguan, China, 3816	July	November	0.015	Flask	High mountain	Sparse vegetation and arid and semiarid grassland
	Ulaan Uul, Mongolia, 1007	December–January	June–July	0.03	Flask	Boreal	
	Tae-ahn Peninsula, Korea, 16	March, September	July	0.04	Flask	Humid continental	
	Mauna Loa, Hawaii, 3397	November	August	0.031	Flask	High mountain	
Kong et al. (2010), taken from Liu et al. (2004)	Mt. Waliguan, China, 3816	July	April	0.04		High mountain	Sparse vegetation and arid and semiarid grassland
Vermeulen et al. (2011)	Cabaw, The Netherlands, −0.7	January	June, August	<0.15	20–200	Atlantic with soft summer	Intensively and extensively managed grassland
Zhang et al. (2013)	Mt. Waliguan, China, 3816	August	November	<0.015	80	High mountain	Sparse vegetation and arid and semiarid grassland
	Mauna Loa, Hawaii, 3397	November	August	<0.035	11.5	High mountain	
	Niwot Ridge, Colorado, 3523	December	July	<0.035		High mountain	
	Schneefernerhaus, Germany, 2671	April, August	June, November	<0.02		Tundra	Rock
Zhou et al. (2004)	Mt. Waliguan, China, 3816	June–August	December	<0.01	80	High mountain	Sparse vegetation and arid and semiarid grassland

3.2. Incremental changes

Following Tiwari et al. (2013), variability of both trace gases was studied with the day-to-day incremental changes calculated as $(\sum_{t=2}^{n} C(t) - C(t-1))/(n-1)$. In this paper, C is the smoothed concentration and n the number of days in the month. Values obtained are represented in Fig. 5. As at Cape Rama, four alternate periods may be observed. However, their times are different as are the features of the site, leading to higher values at CIBA. Daily CO_2 increase was from February to April, when vegetation develops in late winter, and after winter, and particularly from September to December, when vegetation and soil activities begin their cycle after the hot summer. A decrease in CO_2 was noticeable from May to August accompanied by the decline in vegetation activity and the expansion of the boundary layer in summer. Following the annual evolution, only two periods were observed for CH_4, with incremental changes being negative during the first half of the year and positive in the second half, and proving extremely low in both intervals.

3.3. Second order harmonic model

Harmonic models have been used in different papers, and are part of an equation in which the other part is a polynomial of time. The number of harmonics varies, although three (Eneroth et al., 2005; Higuchi et al., 2003; Inoue et al., 2006) and four (Vermeulen et al., 2011) harmonics are frequent. In the present paper, taking into account the irregular distribution of the annual cycle presented by the kernel estimation, only two harmonics were used due to the model's simplicity and the satisfactory agreement with observations.

Coefficients of the second order model were calculated and are presented in Table 5. Coefficient a represents the average concentration of the harmonic function given by Eq. (5), which shows slight differences for CO_2 at the three levels and is very similar for CH_4.

Coefficients b and c represent the amplitudes of the annual and half-annual cycles, respectively. Both were similar, although one hundredth that of a for CO_2, revealing that cycle amplitudes were small compared to the average value, with the half-annual cycle amplitude being slightly lower than for the annual cycle. The maximum of the annual cycle was located near early March and the minimum in early September, following θ_1. However, the half-annual cycle showed maxima in mid May and November and minima in mid February and August. Addition of both harmonic functions was strengthened in August, accounting for the significant minimum observed during this month.

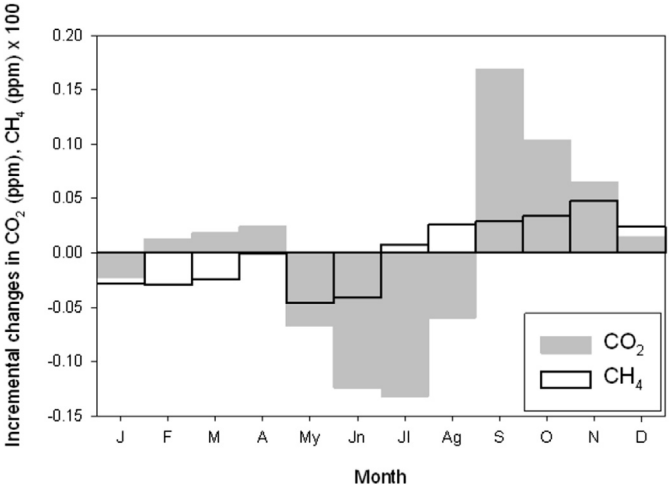

Fig. 5. Daily incremental changes obtained from the smoothed concentration of both trace gases.

Table 5
Coefficients of Eq. (5) and correlation coefficients between the kernel estimation and the second order model.

Gas	Level (m)	a (ppm)	b (ppm)	θ_1 (days)	c (ppm)	θ_2 (days)	r
CO_2	1.8	401.3	4.6	62	3.7	136	0.976
	3.7	400.3	4.5	60	3.3	137	0.984
	8.3	399.1	4.5	56	2.8	139	0.990
CH_4	1.8	1.8982	0.0231	14	0.0043	145	0.983
	3.7	1.8990	0.0229	13	0.0043	144	0.983
	8.3	1.8993	0.0226	13	0.0041	143	0.982

The amplitude of the annual CH_4 cycle was about a hundredth of the average value, indicating that this evolution was also very slight against the average value. However, the amplitude of the half-annual cycle was one fifth of the annual cycle amplitude, revealing that this cycle had less weight. Maxima were in mid January for the annual cycle and late May and November for the half-annual cycle, and minima occurred in mid July for the annual cycle and late February and August for the half-annual cycle, thus determining a more marked evolution than that obtained with only one harmonic function.

Mean percentage differences between observations and smoothed values were similar to those calculated by the kernel procedure for both gases. Finally, the correlation coefficient between values calculated with both the kernel and the harmonic model proved satisfactory.

4. Conclusions

The kernel estimation of the cycle provided more detailed information about changes of the annual evolution than the second order harmonic model did.

Daily and short term oscillations were satisfactorily avoided in the kernel estimation. Depending on their response to window width, two groups of variables were formed. A 10-day window was used for CO_2, NDVI, temperature, and boundary layer height, and 15 days for CH_4 and wind speed.

A vertical gradient of −3.5 ppm in 10 m was observed for CO_2, against a value of 0.0016 ppm for CH_4. Both were linked to local dynamics of the planetary boundary layer.

Two periods corresponding to excess and deficit were observed. The deficit period for CO_2 was shorter, although its concentration trough was more pronounced than for CH_4, whose excess and deficit periods lasted a similar length of time. Day-to-day concentration changes were more noticeable for CO_2.

Vegetation was particularly vigorous at this Mediterranean site from April to June. Photosynthesis contribution seems to be noticeable from mid May to early July. Low CO_2 during summer was attributed to weak plant activity and expansion of the planetary boundary layer. Background evolution contribution should also be the subject of specific analysis.

The successful correlation between annual CH_4 evolution and meteorological variables reveals that the meteorological conditions have a major impact on this cycle.

The second order model is simple and ensures an irregular interval between maximum and minimum. Amplitudes of harmonics used were similar for CO_2, indicating comparable weight of annual and half-annual periods. However, the annual amplitude was five times greater than the half-annual amplitude for CH_4, revealing the secondary influence of this cycle.

Finally, a further analysis of trends will be improved with the procedures employed in this paper in order to gain a better description of how both gases evolve.

Conflict of interests

The authors declare that there is no conflict of interests regarding publication of this paper.

Acknowledgements

The authors wish to acknowledge the financial support of the Ministry of Economy and Competitiveness and ERDF funds (grant numbers CGL2009-11979 and CGL2014-53948-P).

References

Anderson-Cook, C.M., Noble, R.B., 2001. An alternate model for cylindrical data. Nonlinear. Anal. 47, 2011–2022.
Anderson-Cook, C.M., 2000. A second order model for cylindrical data. J. Stat. Comput. Simul. 66, 51–65.
Artuso, F., Chamard, P., Piacentino, S., Sferlazzo, D.M., De Silvestri, L., di Sarra, A., Meloni, D., Monteleone, F., 2009. Influence of transport and trends in atmospheric CO_2 at Lampedusa. Atmos. Environ. 43, 3044–3051.
Artuso, F., Chamard, P., Piacentino, S., di Sarra, A., Meloni, D., Monteleone, F., Sferlazzo, D.M., Thiery, F., 2007. Atmospheric methane in the Mediterranean: analysis of measurements at the island of Lampedusa during 1995–2005. Atmos. Environ. 41, 3877–3888.
Atlas Agroclimático de Castilla y León-ITACYL-AEMET, 2013. http://atlas.itacyl.es, (accessed in January 2016).
Bakwin, P.S., Tans, P.P., Zhao, C., Ussler III, W., Quesnell, E., 1995. Measurements of carbon dioxide on a very tall tower. Tellus Ser. B 47 B, 535–549.
Bakwin, P.S., Tans, P.P., Hurst, D.F., Zhao, C., 1998. Measurements of carbon dioxide on very tall towers: results of the NOAA/CMDL program. Tellus, Ser. B Chem. Phys. Meteorol. 50, 401–415.
Boeckx, P., Van Cleemput, O., 2001. Estimates of N_2O and CH_4 fluxes from agricultural lands in various regions in Europe. Nutr. Cycl. Agroecosyst. 60, 35–47.
Buragiene, S., Šarauskis, E., Romaneckas, K., Sasnauskiene, J., Masilionyte, L., Kriauciuniene, Z., 2015. Experimental analysis of CO_2 emissions from agricultural soils subjected to five different tillage systems in Lithuania. Sci. Total Environ. 514, 1–9.
Chen, H., Winderlich, J., Gerbig, C., Hoefer, A., Rella, C.W., Crosson, E.R., Van Pelt, A.D., Steinbach, J., Kolle, O., Beck, V., Daube, B.C., Gottlieb, E.W., Chow, V.Y., Santoni, G.W., Wofsy, S.C., 2010. High-accuracy continuous airborne measurements of greenhouse gases (CO_2 and CH_4) using the cavity ring-down spectroscopy (CRDS) technique. Atmos. Meas. Tech. 3, 375–386.
Cheng, Y.L., Aa, X.Q., Yun, F.H., Zhou, L.X., Liu, L.X., Fang, S.X., Xu, L., 2013. Simulation of CO_2 variations at Chinese background atmospheric monitoring stations between 2000 and 2009: applying a CarbonTracker model. Chin. Sci. Bull. 58, 3986–3993.
Crosson, E.R., 2008. A cavity ring-down analyzer for measuring atmospheric levels of methane, carbon dioxide, and water vapor. Appl. Phys. B 92, 403–408.
Donnelly, A., Misstear, B., Broderick, B., 2011. Application of nonparametric regression methods to study the relationship between NO_2 concentrations and local wind direction and speed at background sites. Sci. Total Environ. 409, 1134–1144.
Eneroth, K., Aalto, T., Hatakka, J., Holmén, K., Laurila, T., Viisanen, Y., 2005. Atmospheric transport of carbon dioxide to a baseline monitoring station in northern Finland. Tellus B 57, 366–374.
Evrendilek, F., Ben-Asher, J., Aydin, M., Çelik, I., 2005. Spatial and temporal variations in diurnal CO_2 fluxes of different Mediterranean ecosystems in Turkey. J. Environ. Monit. 7, 151–157.
García, M.A., Sánchez, M.L., Pérez, I.A., 2012. Differences between carbon dioxide levels over suburban and rural sites in Northern Spain. Environ. Sci. Pollut. Res. 19, 432–439.
Haszpra, L., Barcza, Z., Szilágyi, I., Dlugokencky, E., Tans, P., 2011. Trends and temporal variations of major greenhouse gases at a rural site in central Europe. In: Haszpra, L. (Ed.), Atmospheric Greenhouse Gases: the Hungarian Perspective. Springer, Dordrecht, pp. 29–47.
Haszpra, L., Barcza, Z., Hidy, D., Szilágyi, I., Dlugokencky, E., Tans, P., 2008. Trends and temporal variations of major greenhouse gases at a rural site in Central Europe. Atmos. Environ. 42, 8707–8716.
Henry, R.C., Vette, A., Norris, G., Vedantham, R., Kimbrough, S., Shores, R.C., 2011. Separating the air quality impact of a major highway and nearby sources by nonparametric trajectory analysis. Environ. Sci. Technol. 45, 10471–10476.
Henry, R.C., Chang, Y.S., Spiegelman, C.H., 2002. Locating nearby sources of air pollution by nonparametric regression of atmospheric concentrations on wind direction. Atmos. Environ. 36, 2237–2244.
Hernández-Paniagua, I.Y., Lowry, D., Clemitshaw, K.C., Fisher, R.E., France, J.L., Lanoisellé, M., Ramonet, M., Nisbet, E.G., 2015. Diurnal, seasonal, and annual trends in atmospheric CO_2 at southwest London during 2000–2012: wind sector analysis and comparison with Mace Head, Ireland. Atmos. Environ. 105, 138–147.
Higuchi, K., Worthy, D., Chan, D., Shashkov, A., 2003. Regional source/sink impact on the diurnal, seasonal and inter-annual variations in atmospheric CO_2 at a boreal forest site in Canada. Tellus B 55, 115–125.
ICGC (Mapping and Geological Institute of Catalonia), 2016. http://www.icc.cat/, (accessed in January 2016).
Inoue, H.Y., Matsueda, H., Igarashi, Y., Sawa, Y., Wada, A., Nemoto, K., Sartorius, H., Schlosser, C., 2006. Seasonal and long-term variations in atmospheric CO_2 and ^{85}Kr in Tsukuba, central Japan. J. Meteorol. Soc. Jpn. 84, 959–968.
Kim, D.G., Kirschbaum, M.U.F., 2015. The effect of land-use change on the net exchange rates of greenhouse gases: a compilation of estimates. Agric. Ecosys. Environ. 208, 114–126.
Kim, H.S., Chung, Y.S., Tans, P.P., Dlugokencky, E.J., 2015. Decadal trends of atmospheric methane in East Asia from 1991 to 2013. Air Qual. Atmos. Health 8, 293–298.
Kong, S.F., Lu, B., Han, B., Bai, Z.P., Xu, Z., You, Y., Jin, L.M., Guo, X.Y., Wang, R., 2010. Seasonal variation analysis of atmospheric CH_4, N_2O and CO_2 in Tianjin offshore area. Sci. China Earth Sci. 53, 1205–1215.
Lintner, B.R., Buermann, W., Koven, C.D., Fung, I.Y., 2006. Seasonal circulation and Mauna Loa CO_2 variability. J. Geophys. Res. 111, D13104. http://dx.doi.org/10.1029/2005JD006535.
Liu, M., Wu, J., Zhu, X., He, H., Jia, W., Xiang, W., 2015. Evolution and variation of atmospheric carbon dioxide concentration over terrestrial ecosystems as derived from eddy covariance measurements. Atmos. Environ. 114, 75–82.
Liu, Q., Wang, Y.S., Wang, M.X., 2004. Seasonal variations of atmospheric greenhouse gases in Beijing. Adv. Earth Sci. 19, 817–822 (in Chinese).
Luyssaert, S., Abril, G., Andres, R., Bastviken, D., Bellassen, V., Bergamaschi, P., Bousquet, P., Chevallier, F., Ciais, P., Corazza, M., Dechow, R., Erb, K.H., Etiope, G., Fortems-Cheiney, A., Grassi, G., Hartmann, J., Jung, M., Lathière, J., Lohila, A., Mayorga, E., Moosdorf, N., Njakou, D.S., Otto, J., Papale, D., Peters, W., Peylin, P., Raymond, P., Rödenbeck, C., Saarnio, S., Schulze, E.D., Szopa, S., Thompson, R., Verkerk, P.J., Vuichard, N., Wang, R., Wattenbach, M., Zaehle, S., 2012. The European land and inland water CO_2, CO, CH_4 and N_2O balance between 2001 and 2005. Biogeosciences 9, 3357–3380.
MAGRAMA (Ministry of Agriculture, Food and Environment), 2016. http://eportal.magrama.gob.es/websiar/, (accessed in January 2016).
Metzger, M.J., Bunce, R.G.H., Jongman, R.H.G., Mücher, C.A., Watkins, J.W., 2005. A climatic stratification of the environment of Europe. Glob. Ecol. Biogeogr. 14, 549–563.
Myneni, R.B., Tucker, C.J., Asrar, G., Keeling, C.D., 1998. Interannual variations in satellite-sensed vegetation index data from 1981–1991. J. Geophys. Res. 103, 6145–6160.
Nakazawa, T., Ishizawa, M., Higuchi, K., Trivett, N.B.A., 1997. Two curve fitting methods applied to CO_2 flask data. Environmetrics 8, 197–218.
NASA, 2016. https://earthdata.nasa.gov/ (accessed in January 2016).
NASA, 2000. http://earthobservatory.nasa.gov/Features/MeasuringVegetation/ (accessed in January 2016).
NOAA, 2016. http://www.esrl.noaa.gov/gmd/ccgg/flask.php accessed in May 2016).
Pérez, I.A., Sánchez, M.L., García, M.A., Ozores, M., Pardo, N., 2015a. Cluster analysis applied to CO_2 concentrations at a rural site. Environ. Sci. Pollut. Res. 22, 1954–1962.
Pérez, I.A., Sánchez, M.L., García, M.A., Pardo, N., 2015b. Analysis of air mass trajectories in the northern plateau of the Iberian Peninsula. J. Atmos. Sol.-Terr. Phys. 134, 9–21.
Pérez, I.A., Sánchez, M.L., García, M.A., Pardo, N., 2013. Carbon dioxide at an unpolluted site analysed with the smoothing kernel method and skewed distributions. Sci. Total Environ. 456–457, 239–245.
Pérez, I.A., Sánchez, M.L., García, M.A., 2012. CO_2 dilution in the lower atmosphere from temperature and wind speed profiles. Theor. Appl. Climatol. 107, 247–253.
Pérez, I.A., García, M.A., Sánchez, M.L., de Torre, B., 2007. Analysis of directional meteorological data by means of cylindrical models. Renew. Energy 32, 459–473.
Pérez-Hoyos, A., Martínez, B., García-Haro, F.J., Moreno, A., Gilabert, M.A., 2014. Identification of ecosystem functional types from coarse resolution imagery using a self-organizing map approach: a case study for Spain. Remote Sens. 6, 11391–11419.
Pu, J.J., Xu, H.H., He, J., Fang, S.X., Zhou, L.X., 2014. Estimation of regional background concentration of CO_2 at Lin'an Station in Yangtze River Delta, China. Atmos. Environ. 94, 402–408.
Rella, C., 2010. Accurate Greenhouse Gas Measurements in Humid Gas Streams using the Picarro G1301 Carbon dioxide/Methane/Water Vapor Gas Analyzer. Available from: http://www.picarro.com/assets/docs/White_Paper_G1301_Water_Vapor_Correction.pdf.
Rella, C.W., Chen, H., Andrews, A.E., Filges, A., Gerbig, C., Hatakka, J., Karion, A., Miles, N.L., Richardson, S.J., Steinbacher, M., Sweeney, C., Wastine, B., Zellweger, C., 2013. High accuracy measurements of dry mole fractions of carbon dioxide and methane in humid air. Atmos. Meas. Tech. 6, 837–860.
Saha, S., Chakraborty, D., Sehgal, V.K., Pal, M., 2015. Potential impact of rising atmospheric CO_2 on quality of grains in chickpea (*Cicer arietinum* L.). Food. Chem. 187, 431–436.
Sánchez, M.L., García, M.A., Pérez, I.A., Pardo, N., 2014. CH_4 continuous measurements in the upper Spanish plateau. Environ. Monit. Assess. 186, 2823–2834.

Sepulveda-Jauregui, A., Walter Anthony, K.M., Martinez-Cruz, K., Greene, S., Thalasso, F., 2015. Methane and carbon dioxide emissions from 40 lakes along a north–south latitudinal transect in Alaska. Biogeosciences 12, 3197–3223.

Tans, P.P., Thoning, K.W., Elliott, W.P., Conway, T.J., 1989. Background atmospheric CO_2 patterns from weekly flask samples at Barrow, Alaska: optimal signal recovery and error estimates. NOAA Tech. Mem. ERL ARL-173 112–123.

Tian, X., Xie, Z., Liu, Y., Cai, Z., Fu, Y., Zhang, H., Feng, L., 2014. A joint data assimilation system (Tan-Tracker) to simultaneously estimate surface CO_2 fluxes and 3-D atmospheric CO_2 concentrations from observations. Atmos. Chem. Phys. 14, 13281–13293.

Thoning, K.W., Tans, P.P., Komhyr, W.D., 1989. Atmospheric carbon dioxide at Mauna Loa Observatory. 2. Analysis of the NOAA GMCC data, 1974–1985. J. Geophys. Res. 94, 8549–8565.

Tiwari, Y.K., Revadekar, J.V., Ravi Kumar, K., 2013. Variations in atmospheric carbon dioxide and its association with rainfall and vegetation over India. Atmos. Environ. 68, 45–51.

Tucker, C.J., Slayback, D.A., Pinzon, J.E., Los, S.O., Myneni, R.B., Taylor, M.G., 2001. Higher northern latitude normalized difference vegetation index and growing season trends from 1982 to 1999. Int. J. Biometeorol. 45, 184–190.

Uglietti, C., Leuenberger, M., Brunner, D., 2011. European source and sink areas of CO_2 retrieved from Lagrangian transport model interpretation of combined O_2 and CO_2 measurements at the high alpine research station Jungfraujoch. Atmos. Chem. Phys. 11, 8017–8036.

Vermeulen, A.T., Hensen, A., Popa, M.E., Van Den Bulk, W.C.M., Jongejan, P.A.C., 2011. Greenhouse gas observations from Cabauw Tall Tower (1992–2010). Atmos. Meas. Tech. 4, 617–644.

Wada, A., Sawa, Y., Matsueda, H., Taguchi, S., Murayama, S., Okubo, S., Tsutsumi, Y., 2007. Influence of continental air mass transport on atmospheric CO_2 in the western North Pacific. J. Geophys. Res. 112, D07311. http://dx.doi.org/10.1029/2006JD007552.

Wageningen UR, 2016. http://www.wageningenur.nl/en/Expertise-Services/Research-Institutes/alterra/Projects/EBONE-2/Products/European-Environmental-Stratification.htm (accessed in January 2016).

WDCGG (World Data Centre for Greenhouse Gases), 2016. http://ds.data.jma.go.jp/gmd/wdcgg/ (accessed in January 2016).

Zhang, F., Zhou, L.X., Xu, L., 2013. Temporal variation of atmospheric CH_4 and the potential source regions at Waliguan, China. Sci. China Earth Sci. 56, 727–736.

Zeng, J., Matsunaga, T., Mukai, H., 2010. METEX - a flexible tool for air trajectory calculation. Environ. Modell. Softw. 25, 607–608.

Zhou, L., Conway, T.J., White, J.W.C., Mukai, H., Zhang, X., Wen, Y., Li, J., MacClune, K., 2005. Long-term record of atmospheric CO_2 and stable isotopic ratios at Waliguan Observatory: background features and possible drivers, 1991–2002. Glob. Biogeochem. Cycles 19, GB3021. http://dx.doi.org/10.1029/2004GB002430.

Zhou, L.X., Worthy, D.E.J., Lang, P.M., Ernst, M.K., Zhang, X.C., Wen, Y.P., Li, J.L., 2004. Ten years of atmospheric methane observations at a high elevation site in Western China. Atmos. Environ. 38, 7041–7054.

Zhu, C., Yoshikawa-Inoue, H., 2015. Seven years of observational atmospheric CO_2 at a maritime site in northernmost Japan and its implications. Sci. Total Environ. 524–525, 331–337.